Ocean Dynamics (2010) 60:81–91
DOI 10.1007/s10236-009-0244-z

Seasonality and anomalies of sea surface temperature off the coast of Nayarit, Mexico

Emilio Palacios-Hernández · Laura E. Carrillo · Anatoliy Filonov · Luis Brito-Castillo · Carlos E. Cabrera-Ramos

Received: 19 March 2009 / Accepted: 5 November 2009 / Published online: 28 November 2009

Abstract Sea surface temperature (SST) harmonic and empirical orthogonal function (EOF) analyses covering 18 years were performed for the area located from 114° to 105° W and from 18° to 25° N. The results indicate that the influence of the annual signal predominates over the semi-annual signal, and the closer to the coast, the stronger the annual harmonic. Several interannual anomalies arose that are connected with the main global indexes, especially the Oceanic Niño Index. Pearson correlations between the first temporal mode of the SST and regional rainfalls in Nayarit indicate that maximum correlations (r>0.7) are observed when there is a +1-month lag between the series. However, this result indicates that SST is delayed with 1 month after rainfall occurrence, which shows that the dominant influence in this relationship is not the SST forcing.

Keywords Nayarit · Rainfall · SST

Responsible Editor: Franciscus Colijn

E. Palacios-Hernández · A. Filonov · L. Brito-Castillo
Universidad de Guadalajara,
Revolución 1500, Col. Olímpica, Guadalajara,
Jalisco 44840, Mexico

L. E. Carrillo
El Colegio de la frontera Sur,
Av. Centenario, Km. 5.5. Cd. Chetumal,
Quintana Roo 77014, Mexico

L. Brito-Castillo (✉)
Centro de Investigaciones Biológicas del Noroeste (CIBNOR),
Unidad Sonora, Campus Guaymas, Estero de Bacochibampo,
Guaymas,
Sonora 85454, Mexico
e-mail: lbrito04@cibnor.mx

C. E. Cabrera-Ramos
Centro de Investigación Científica y de Educación
Superior de Ensenada,
Km. 107 Carretera Tijuana-Ensenada, Ensenada,
Baja California 22860, Mexico

1 Introduction

Sea surface temperature (SST) data obtained by satellite infrared images are often used for the calculation of latent and sensible heat flows (Curry and Webster 1999), as a passive tracer of currents (Palacios-Hernandez et al. 1996), climatic studies (Meza 2006; Lavín et al. 2003), and prognoses of the ocean–atmosphere interaction (Enfield 1996; Enfield and Mayer 1997; Hernández 2002; Meza 2006). These data are of great importance in most environmental studies as a dominant indicator of climate change. Using data of SST anomalies allows the identification of different weather and oceanographic phenomena.

El Niño-Southern Oscillation (ENSO) is one of the most significant patterns of interannual variability worldwide, and SST is one of the main tracers that distinguish this pattern through positive anomalies (Wang and Fiedler 2006). In Mexico, the effects of El Niño appear in the rise of water temperature, sea level, and the interannual variations of weather conditions of practically the entire western Mexican coast (Martínez 2006). Other causes of SST variations exist, such as “La Niña” and the oscillations of the South Pacific and the North Pacific high-pressure centers.

For a few decades, high-resolution SST data are available from satellites. Researchers have used SST data from the Eastern Tropical Pacific to analyze ENSO events (Wang and Fiedler 2006), climatic changes, inter-decadal variability (Mestas-Nuñez and Miller 2006), atmospheric

forcings (Amador et al. 2006), and general oceanography of this region (Wyrtki 1964, 1965a, b, 1966, 1967). Other studies have analyzed separately smaller sections of the area, as is the case of Hernández (2002) for Cuba, Lavín et al. (2003) for the Gulf of California, and Martínez (2006) for the Mexican Central Pacific coast.

At present, oceanographic studies along the Mexican coasts are increasing, but these studies only marginally have considered a SST climatic description for specific areas. Such investigations are very useful in clarifying the link between ocean and atmosphere interaction and for understanding rainfall over the continent.

This paper provides a SST climatic description off the coasts of Nayarit, Jalisco, southern Sinaloa, and the Southern Gulf of California (central coast of the Mexican Pacific) and clarifies the link between SST in this region and rainfall in Nayarit. For these analyses, an 18-year series (1983–2000) of infrared satellite images and monthly average rainfall for Nayarit during the same period were used. Causes of interannual anomalies of the SST are discussed.

2 Study area

The study area is in the Pacific Ocean from 114° to 105° W and from 18° to 25° N (Fig. 1) and extends over the coasts of the federal states of Nayarit, Jalisco, central and southern Sinaloa, and the southern Baja California Peninsula. This area corresponds to the northern portion of the Eastern Tropical Pacific (Trasviña et al. 1999).

Northwest of the area, the average annual SST is 21°C, while in the South, it is 27°C (Shea et al. 1992). The lowest SST (~18°C) occurs from January through March, and the highest (~30°C) occurs between July and September (da Silva et al. 1994). Normal average temperature reaches 28°C (Shea et al. 1992). Most of the area has ocean depths between 2,000 and 3,000 m.

According to Wyrtki (1965b), the Southwest Mexican coastal current (Mexican current) between the Gulf of Tehuantepec (Oaxaca) and Cabo Corrientes (Jalisco) is an important part of the pattern of ocean currents in the Eastern Tropical Pacific (Lavín et al. 2006). Wyrtki (1965b) stated that in June and July, the flow reached to Cabo Corrientes. This coastal current at Cabo Corrientes and around the Islas Marias has a velocity of ~8 cm/s. An eddy departs from the Mexican current and enters the Gulf of California (Zamudio et al. 2007). From the north, the California Current influences the area, carrying cold waters into this region. Lavín et al. (2006) state that this current is introduced into the coastal current by eddies and the Mexican current during summer.

3 Materials and methods

AVHRR satellite data from the Jet Propulsion Laboratory Physical Oceanography Distributed Active Archive Center

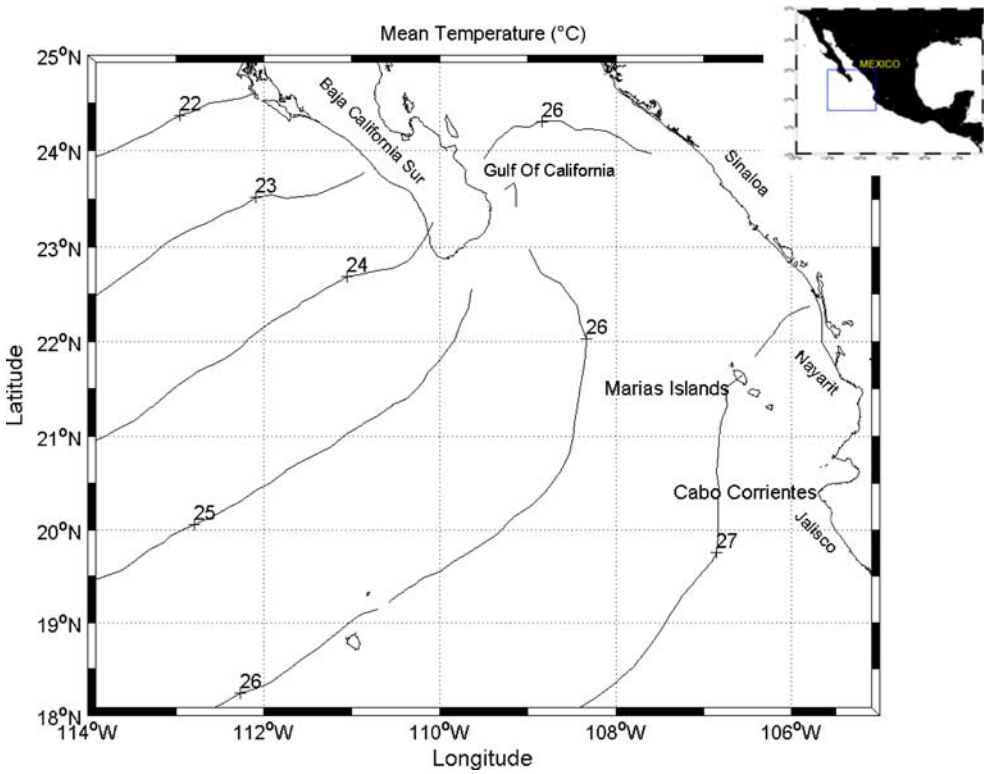

Fig. 1 Mean temperature and study area

(http://podaac.jpl.nasa.gov) were used. Images with a 18×18-km pixel resolution from every eighth day were used (a total of 930 images between January 1983 and October 2000). From each image, a matrix of SST data covering the study area was extracted (Cabrera-Ramos 2005). Images were analyzed separately, discarding those with clouds, lack of data, or erroneous information, like temperature above the expected (50°C).

From the resulting matrix, which consisted of 41×53 pixels, monthly averages were computed. Where an image covering a complete month was discarded, a linear interpolation procedure was made using information from previous and later months. Monthly averages were used to compute the temporal average ($\overline{T}(x,y)$) of the series:

$$\overline{T}(x,y) = \frac{1}{N}\sum_{j=1}^{N} T(x,y,t),$$

where N=214, which is the number of months in the data set. Harmonic analysis was performed, resulting in the extraction of the temporal average at each point and the superposition of the annual and semi-annual signals (Ripa 2002; Lavín et al. 2006).

SST monthly averages were derived by applying empirical orthogonal functional analysis to obtain the temporal modes of the series. The spectral analysis of these temporal modes indicated that the annual and semi-annual signals were the most energetic; therefore, annual and semi-annual signals were extracted to obtain the interannual variability of the series, defined here as anomalies.

Pearson correlation analysis compared SST anomalies and global-scale indices, such as the Southern Oscillation Index (SOI), extratropical Southern Oscillation Index (SOI*), and extratropical Northern Oscillation Index (NOI) (http://www.pfeg.noaa.gov/products/PFEL/modeled/indices), Oceanic Niño Index (ONI; http://ggweather.com/enso/oni.htm), and multivariate ENSO Index (MEI; http://www.cdc.noaa.gov/people/klaus.wolter/MEI). The goal of this analysis was to clarify teleconnections between SST anomalies and large-scale events (for further information about these indexes, see the Appendix). To establish any link between rainfalls in Nayarit and SST in the study area, plot correlation composites were created. Monthly rainfall in Nayarit is calculated as the average monthly totals of climatic stations in Nayarit with the largest correlations (r>0.80) between them. For this study, the information of nine stations were used, all of them located in Nayarit State with codes 18001, 18004, 18009, 18021, 18025, 18028, 18029, 18032, and 18034. The mean monthly as well as minimum and maximum coefficients of correlation between the series are 0.89, 0.83, and 0.96, all of them with p<0.001.

Monthly rainfall totals were extracted from Extractor Rápido de Información Climatológica (ERIC) database created by the Instituto Mexicano de Tecnología del Agua of Mexico to provide a tool for obtaining climatic data of Mexico (ERIC 1996).

4 Results and discussion

4.1 SST harmonic analysis

The annual average SST over the study area is displayed in Fig. 1. Lowest values (21°C) occurred in the northwest, increasing southeastward to a maximum of 27°C near the coast of Jalisco, Nayarit, and southern Sinaloa. This is consistent with the characteristic features reported in the literature, that is, northwestern area is influenced by the California current, characterized by low temperatures and salinities (Fiedler and Talley 2006) and dense cloud cover (Amador et al. 2006), relative to the rest of the area. The southeastward increase in average SST reflects the distribution of insolation (Amador et al. 2006) and the continental influence due to differential heating between land–seawater. This causes a large land–sea thermal contrast (Brown et al. 1989; Gill 1982). The 26°C average SST at the mouth of the Gulf of California is also consistent with data reported by Lavín et al. (2003).

The annual harmonic (Fig. 2) shows amplitudes between 2°C and 2.5°C in the south increasing from the Jalisco coast northwestward and has a maximum of 5°C in the Gulf of California. In the south, the annual signal tends to be smaller because of its location somewhat closer to the Equator (Gill 1982) compared to the Gulf of California where the extreme values of the annual signal occurs throughout the year because it is a semi-enclosed basin surrounded by the Sonoran Desert, well known by the extreme seasonal heating–cooling (Fortin 2002), that increases the SST annual harmonic (Lavín et al. 2003). From the Nayarit coast northwestward, temperatures oscillate from 3°C to 3.5°C. According to the phase (Fig. 2), the annual harmonic displays warming in the mouth of the Gulf of California (mid-September, 8.2- to 8.4-month phase). The warming propagates clockwise, centered at the southernmost tip of the Baja California Peninsula. Later in mid-September (8.6 months), warming reaches as far as the Nayarit coast and by mid-October (9.6 months) reaches the southwestern waters of the Baja California Peninsula. These results are consistent with the report by Fiedler and Talley (2006).

The semi-annual harmonic (Fig. 3) shows amplitudes of 0.2°C close to Islas Marias and off the coast of Nayarit. SST increases northward, reaching a maximum of 1.2°C along the western coast of Baja California Sur. From Figs. 2 and 3, the semi-annual harmonic is almost one order of magnitude smaller than the annual harmonic because its

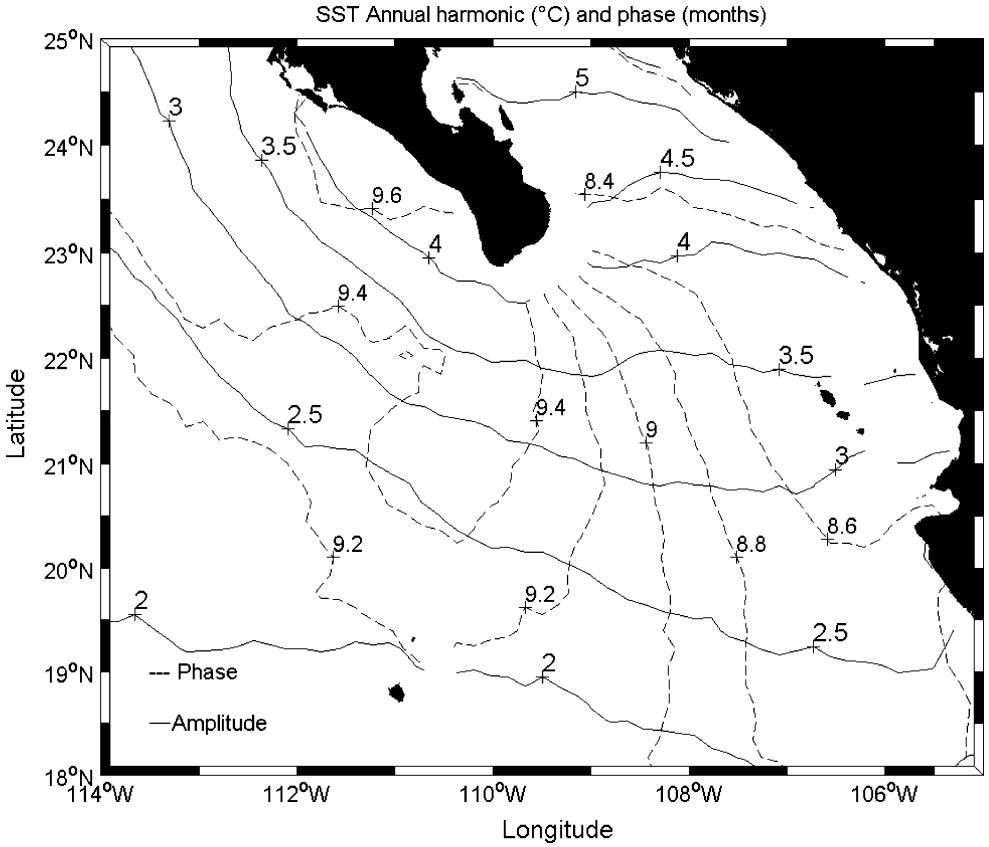

Fig. 2 SST annual harmonic and phase (months)

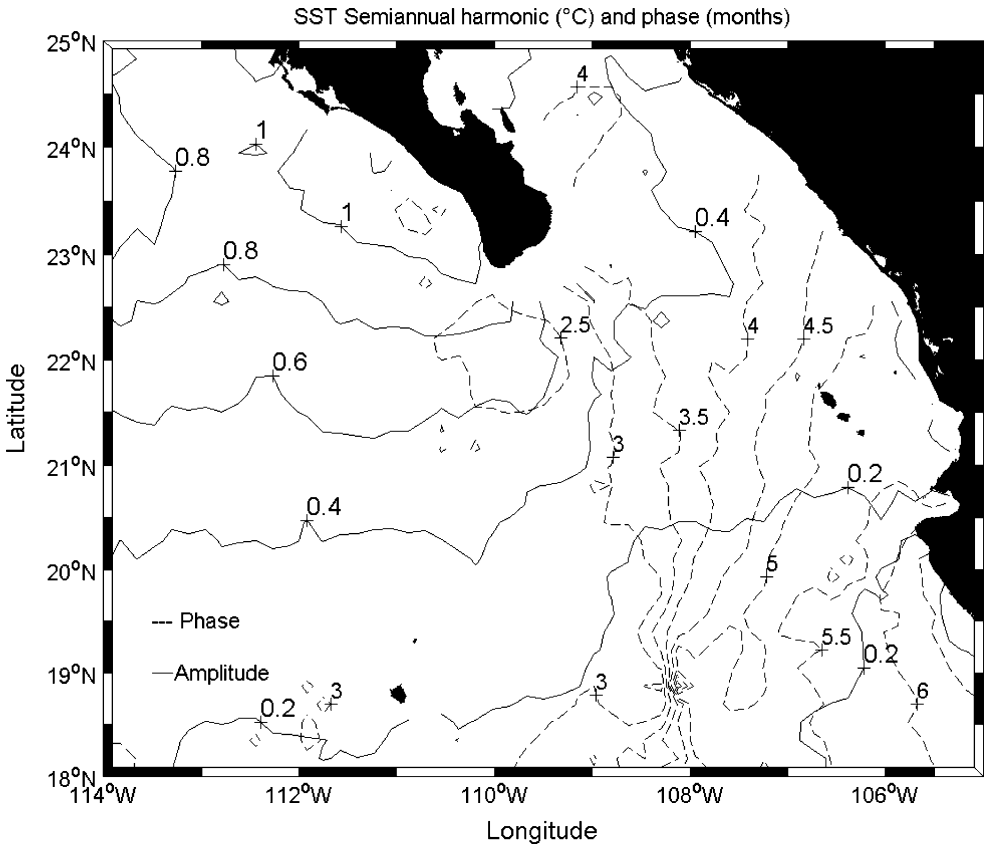

Fig. 3 SST semi-annual harmonic and phase (months)

contribution is relatively small (Fiedler and Talley 2006). The phase of the semi-annual harmonic (Fig. 3) propagates in a NW–SE direction in minimum periods of 2.5 and 3 months (March–April) in the west and a maximum of 6 months off the coast of Jalisco. Along the NW–SE trending coast of Nayarit, the semi-annual harmonic shows a period of 5 months (June).

The percentage of explained variance (EV) of the annual and semi-annual harmonics is displayed in Fig. 4. Explained variance of the order of 90% occurred in the lower Gulf of California, decreasing south–southeastward with values of 85% along the coast of Nayarit and 80% along the coast of Jalisco. Far from these coasts, explained variance diminishes to 70%. Because the annual signal isotherms (Fig. 2) have a similar distribution to the EV, it can be concluded that the most influential signal over the EV is the annual harmonic. The areas away from the equator and close the coast will be more strongly affected by this annual signal (Brown et al. 1989; Gill 1982).

4.2 Empirical orthogonal functions

From the empirical orthogonal functional analysis, the first two modes were retained, which explained 86% and 12% of the variance of the series. Figure 5 displays the first spatial mode, with a value of 1.5 in the south and increasing northwestward to 3.0, with a maximum of 3.5 in the mouth of the Gulf of California. This mode is qualitatively similar to the annual harmonic, as seen in the first temporal mode (Fig. 6a) where the annual signal is dominant. The second spatial mode shows a fan-like distribution with the center at the south end of Baja California Peninsula, with values of 4.0 to the west of the peninsula and −4.0 at the mouth of the Gulf of California. The 0.0 contour follows a north–south orientation close to 108–109° W, which indicates that when the western part of the area is warming, the eastern part is cooling, and vice versa, depending on the value of the second temporal mode (Fig. 6c).

Figure 6a shows the dominance of the annual signal in the first temporal mode, which is also indicated by the spectral analysis (not shown). For this reason, the annual and semi-annual signals (with amplitudes of 1.26°C and 0.14°C, respectively) were extracted from the first mode. The annual and semi-annual signals explain 88% of the variance of the first temporal mode. Replication (modeled) of the first temporal is seen as a heavy line in Fig. 6a. Removing the modeled series from the first temporal mode, we obtained the interannual anomalies, the thin line in Fig. 6b, while the heavy line in this figure displays the smoothed (3-month moving average) interannual anoma-

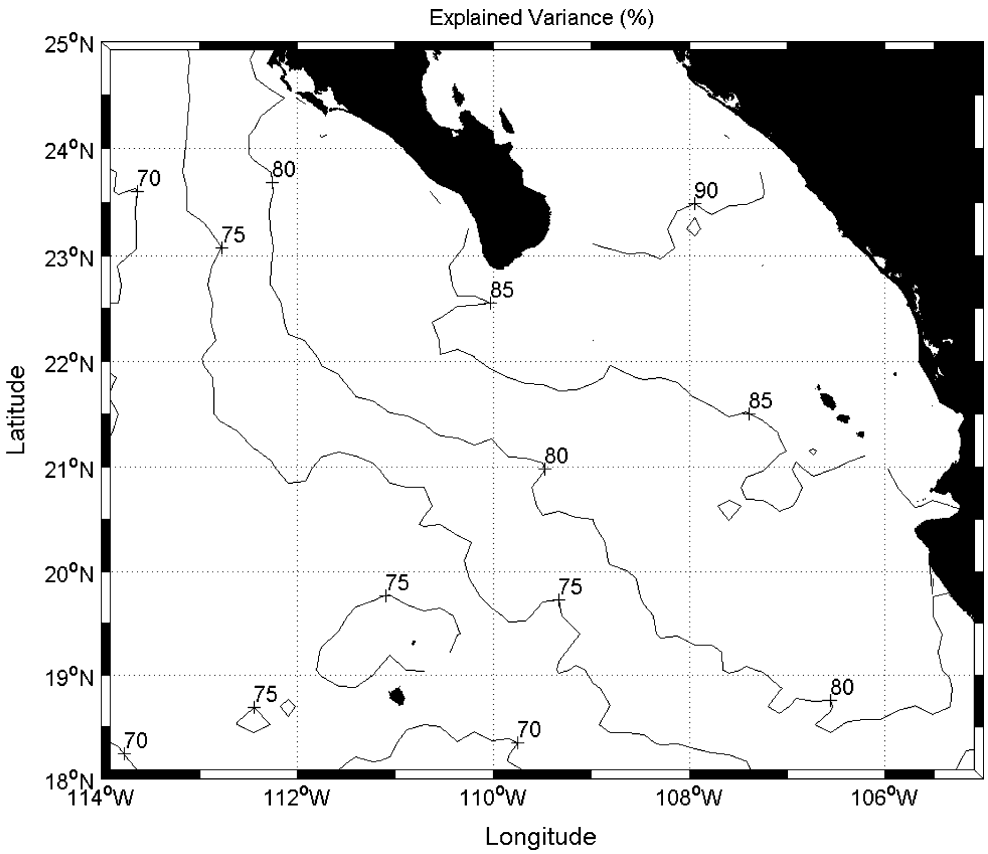

Fig. 4 SST explained variance (%) by the annual and semi-annual harmonics

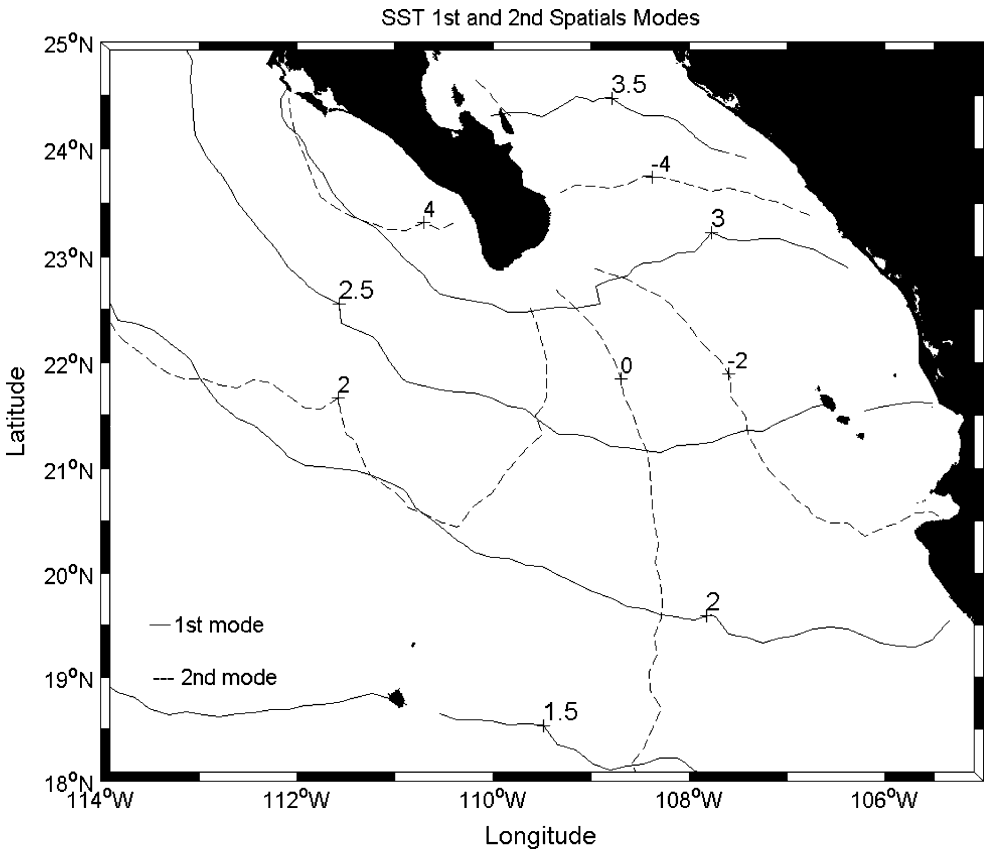

Fig. 5 SST first spatial mode (*continuous line*) and second spatial mode (*dashed line*)

lies; hence, the most intense anomalies can be identified in the study area. A more detailed discussion of this result is given below.

In the second temporal mode, the thin line in Fig. 6c, which is the annual and semi-annual signals, has amplitudes of 0.32°C and 0.14°C, respectively; these are also important. In this case, both signals explained 73% of the variance of this mode. The replica of the second temporal mode shows an annual asymmetry (with positive and negative values) with a duration of negative values lasting 5 months (mid-April to mid-September), whereas positive values lasted 7 months. This asymmetry had been observed before in other oceanographic data within the Northern Gulf of California, for example in the eddy that dominates the circulation in that region (Beier and Ripa 1999; Palacios-Hernández 2001; Palacios-Hernandez et al. 2002; Carrillo et al. 2002) and in SST behavior (Palacios-Hernández et al. 2006) for the same zone.

The annual and semi-annual signals were extracted from the second temporal mode (Fig. 6d, heavy line), so the interannual temperature anomalies can be studied (Fig. 6d, thin line). In this case, the same smoothing as for the first temporal mode was applied (Fig. 6d, heavy line). The most obvious anomalous events occurred in 1983 (+0.3°C), 1989 (−0.3°C), 1991 (−0.3°C), 1992 (+0.3°C), 1998 (+0.3°C), and 1999 (−0.3°C). Since these events are consistent with the interannual anomalies seen in the first temporal mode, they will not be analyzed here.

4.3 Interannual anomalies

The ENSO events are the strongest forcing over the SST interannual variability, so a correlation index must be computed among SST interannual variability given by the first empirical orthogonal function (EOF) temporal mode and these global indexes. Searching the best correlation index value leads to a better understanding on the forecasting of SST interannual anomalies associated with one of the indexes.

Figure 7 shows correlations between the first temporal mode and different global-scale interannual events that affect the central coast of Mexico. This includes lags in different months, up to 1 year before and 1 year later. The horizontal heavy lines in the figure are the 95% confidence levels. Positive correlations between the first temporal mode and the MEI and ONI indices overpass 0.50. The higher positive correlation of 0.55, without phase angle, is between the first mode and the ONI index. Negative correlations were observed between the first mode and the SOI, NOI, and SOI* indices. The

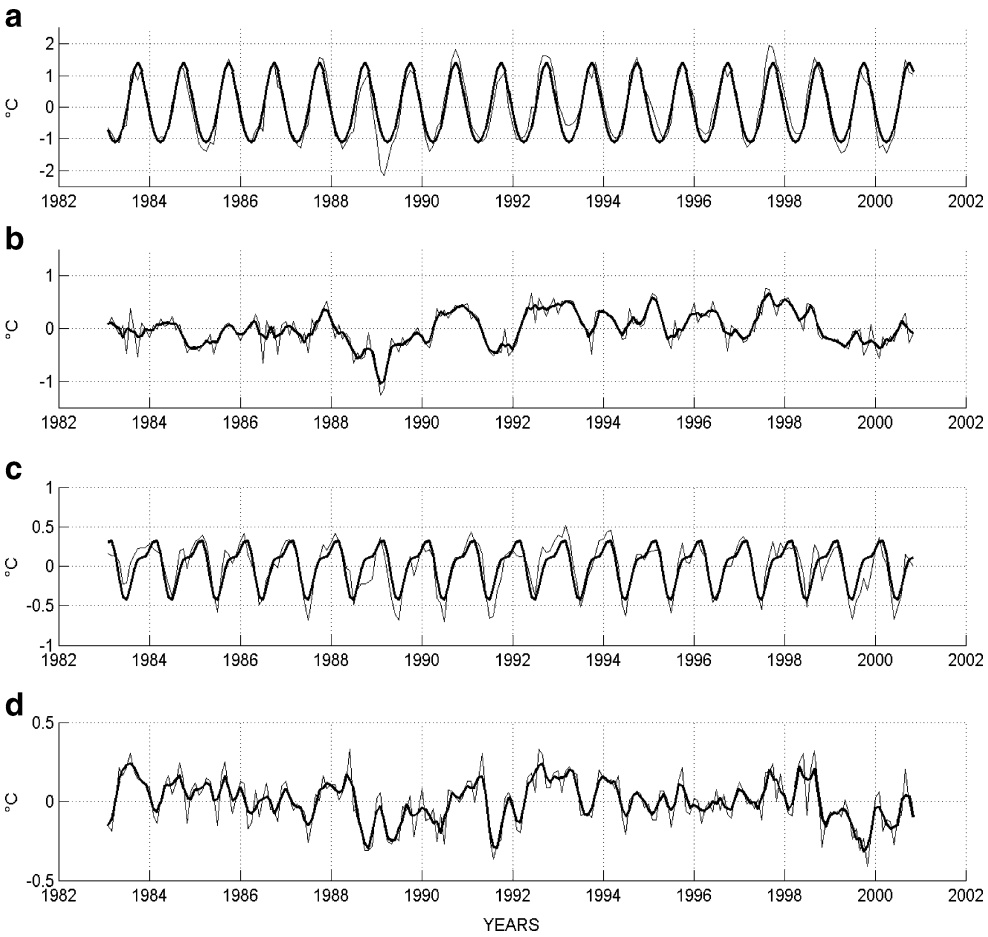

Fig. 6 **a** First temporal SST mode obtained from the EOF's analysis (*thin line*) and modeled by harmonic analysis (*thick line*). **b** SST anomalies obtained by subtracting the modeled first temporal SST mode obtained by harmonic analysis from the first temporal SST mode obtained from the EOF's analysis (*thin line*), *thick line* the same as *thin line* but smoothed with a 3-month moving average. **c** Second temporal SST mode obtained from the EOF's analysis (*thin line*) and modeled by harmonic analysis (*thick line*). **d** SST anomalies obtained by subtracting the modeled second temporal SST mode obtained by harmonic analysis from the second temporal SST mode obtained from the EOF's analysis (*thin line*), *thick line* the same as *thin line* but smoothed with a 3-month moving average

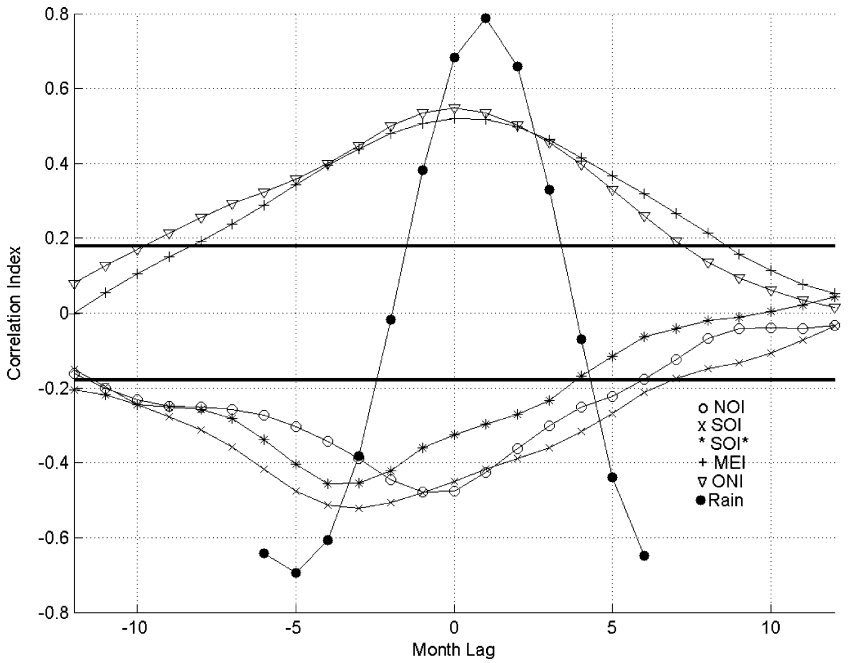

Fig. 7 Correlations between the first temporal mode and various global indices: NOI (*empty circle*), SOI (*ex*), SOI* (*asterisk*), MEI (*plus sign*), ONI (*inverted triangle*), and rainfall (*filled circle*). Values between the lines of ±1.8 are statistically significant ($P<0.05$)

lowest correlation of −0.52 occurred between the first mode and the SOI index, with an absolute maximum lag of 3 months. This result means that the occurrence of a maximum or minimum value of the SOI index affects the SST in the central Mexican Pacific coast 3 months later.

SOI, NOI, and SOIx indexes are evaluated from atmospheric pressure anomalies between Darwin Australia (12°27.683′ S, 130°50.533′ E) and different areas of the Pacific Ocean, whereas the ONI is obtained from the SST anomalies in the 3.4 region of El Niño (i.e., 5° N–5° S, 120°–170° W), while a +1-month delay among these indexes is expected. But it is also known that there are registered events of the ONI that other indexes do not have, like the warm anomaly of the 1994–1995, which, in the other indexes, is barely visible. Meanwhile, the ONI shows this event to be the third event most warm and intense of the whole ONI time series. This affects the coasts of Mexico in a very important way as will shown later in the text.

Figure 7 shows that the MEI and ONI indexes are in phase, although the ONI index shows the best correlation with the first temporal mode, it was selected to explain the interannual anomalies of this mode. In the first temporal mode, larger than 0.5°C absolute anomalies (Fig. 8) occurred in 1989, 1992, 1995, and 1998, with the 1989 anomaly of −1.1°C as the largest anomaly in the series. The 1989 anomaly corresponds to a La Niña. It occurred during the first months of 1989, remarkably cooling the SST of the Gulf of California (Lavín et al. 2003).

The second largest anomaly in the series was 0.7°C occurred at the end of 1997, which occurred with the 1997–1998 El Niño. This El Niño provided the most widespread and remarkable SST of the Mexican central Pacific coast, which was widely documented (Wang and Fiedler 2006).

The third largest absolute SST anomaly (also positive) in the series occurred at the beginning of 1995. In this year, the ONI Index reached 1.25°C, while the SST anomaly was ~0.6°C. The winter of 1994–1995, which coincided with an El Niño, was marked by an anomalous behavior along the Pacific coast of Mexico. Since this particular event generated red tides, a massive cetaceous death (367 dolphins, 8 whales, more than 215 sea birds; PROFEPA 1995) and altered the seasonal circulation of the Northern Golf of California. Apart from resulting in the worst major drought in the south coast of Mexico and the major rainfall in the north coast of Mexico during the decade of the 1990s, finally, the winter of 1994–1995 was the warmest of the decade, which was documented by Delgadillo-Macías et al. (1999), Llunch-Cota et al. (1999), Palacios-Hernández (2001), Lavín et al. (2003), and Palacios-Hernández et al. (2006).

There are other anomalies that deserve attention, although they were weak (less than 0.5°C), for example in 1990 and 1992. In both cases, the first temporal mode showed that the SST was close to 0.5°C and lasted for several months. Lavín et al. (2003) argued that the 1990 SST anomaly was connected with the warm pool of the western hemisphere and was of equatorial origin. Salinas-Zavala et al. (1992) discussed the connection of the 1990

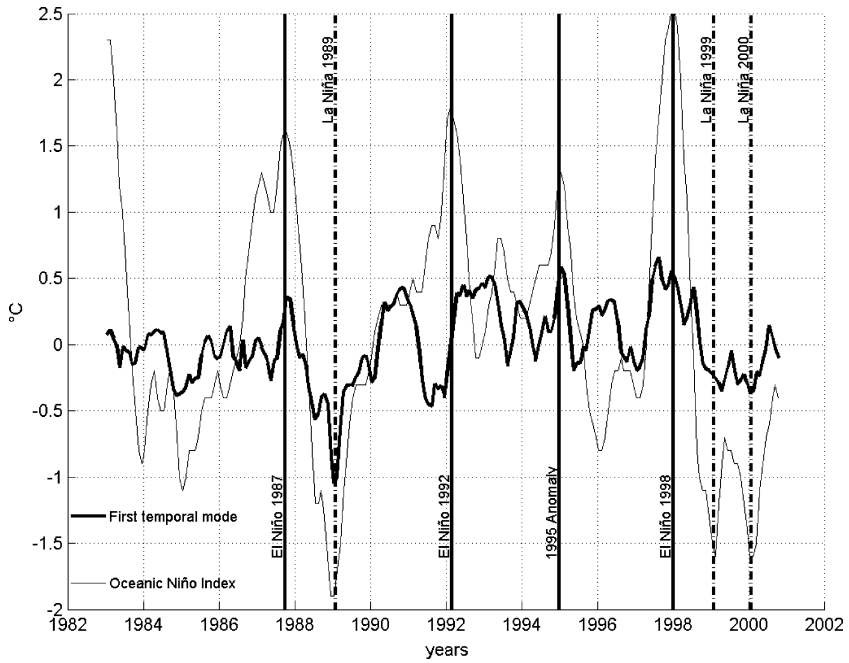

Fig. 8 Comparison between the ONI Index (*thin line*) and the first temporal mode (*thick line*). *Solid lines* are El Niño years and *dashed lines* are La Niña years

SST anomaly with the abundant rainfall in Baja California Sur during the same year. In the case of the 1992 SST anomaly, it coincided with the 1992 El Niño, indicating an equatorial origin. The 1999–2000 La Niña had only a small effect on the SST of the study area. The first temporal mode was close to 0.3°C, which indicated that the relationship between the SST and El Niños and La Niñas in the study area is far from being linear.

4.4 SST vs. rainfall

The correlation between the SST first temporal mode vs. rainfall had different month lags; this is shown in Fig. 7. The highest correlation is with a +1-month lag, that is, a rainfall event occurred before a warming of the SST. Since the best correlation index is obtained with +1-month lag and based on this, a correlation index between the SST time series vs. rainfall totals in Nayarit is displayed in Fig. 9. The results indicate that the largest correlation between SST and rainfall in Nayarit occurred west of Baja California Sur where there is a lag of 1 month (r>0.75).

Although correlations between SST and rainfall in Nayarit are very high (r>0.70), it is not possible to establish a cause–effect relationship since the largest correlations (r>0.75) were delayed 1 month, that is, rainfall occurred first and then seawater temperature increased. Therefore, the contribution of water vapor within the study area for the production of rainfalls in Nayarit does not explain the largest observed correlation. It is necessary to mention that the maximum SST occurs in September, while maximum volume of rain occurs in August, so the peaks between rainfall and SST are out of phase by 1 month with rainfall peaks occurring earlier. The rainfall peak in Nayarit may not only be associated to the seasonal march of SSTs but also to the differential heating between land and ocean (e.g., Turrent and Cavazos 2009). It is not only the warming of the ocean that counts but also the heating of the land. By September, even though the ocean is much warmer than in August, the land is possibly cooler due to August rainfall and other local processes; thus, the land–sea thermal contrast may reverse (possibly strengthening the trades winds; Zuidema et al. 2007), producing less rainfall in September.

5 Conclusions

The central coast of the Mexican Pacific shows a strong annual and semi-annual response, with larger influence of the former (explained variance of 75–90%). Both responses increase northwestward and close to the continent.

This result was reinforced after applying an empirical orthogonal functional analysis that showed that the first

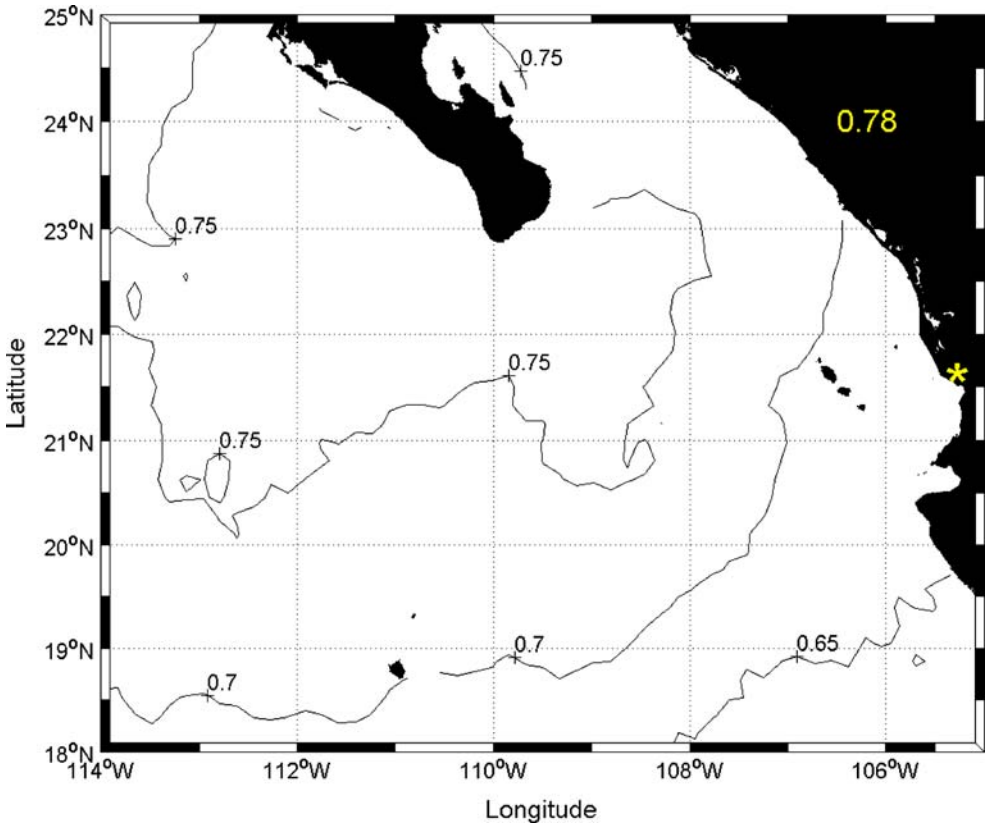

Fig. 9 Correlation index between SST and rain with +1-month time lag (first rain and then rise in temperature). *Correlation point. 0.78 value is the correlation index between the SST first temporal mode and rainfall with a +1-month time lag

temporal mode was strongly correlated with the environmental ONI Index. From the correlation, it was possible to link intense SST anomalies with El Niño and La Niña events. The 1994–1995 and 1997–1998 El Niño events increased SST anomalies more than 0.5°C, and the 1989–1990 La Niña reduced the SST anomaly by about −1.1°C. Other El Niño and La Niña events produced weaker SSTs, a situation implying a nonlinear response.

Since high correlations between rainfall and SST in Nayarit were out of phase by 1 month, it was not possible to establish a cause–effect relationship between the main source of water in the study area and rainfall production in Nayarit.

This study is the first step in clarifying the hydrographic and dynamics of the study area. Although the understanding of land–sea rainfall production for the continent is very important, few oceanographic studies have been made. Only recently, direct observations have been recorded, increasing the detail necessary to study characteristic features of the study area.

Acknowledgments We thank Sergio U. Lillingston-Pérez for assistance and to the anonymous reviewers for their effort. CIBNOR staff edited the English language text. This project was funded by CONACYT grant 44870F, J50757-F and S0013-2006-1-48492.

Appendix

The strength of the El Niño-Southern Oscillation (ENSO) is measured by the Southern Oscillation Index (SOI).The NOI (extratropical-based Northern Oscillation Index) and its analog, the SOI* (extratropical-based Southern Oscillation Index) are new indices of mid-latitude climate fluctuations that show interesting relationships with fluctuations in marine ecosystems and populations. They reflect the variability in equatorial and extratropical teleconnections and represent a wide range of local and remote climate signals. The indices are counterparts to the traditional Southern Oscillation Index (SOI) that relate variability in the atmospheric forcing of climate change in northern and southern mid-latitude hemisphere regions.

The indices are computed from NCEP sea level pressure anomalies (SLPA; monthly sea level pressure minus climatology) of the North Pacific High (NPH; 35° N,130° W), South Pacific High (SPH; 30° S,95° W), Darwin (10° S,130° E), and Tahiti (18° S,150° W). The NOI, SOI*, and SOI are created as follows:

NOI = SLPA_NPH – SLPA_DARWIN

SOI* = SLPA_SPH - SLPA_DARWIN

SOI = SLPA_TAHITI - SLPA_DARWIN

(http://www.pfeg.noaa.gov/products/PFEL/modeled/indices/NOIx/compute.html).

The Oceanic Niño Index (ONI) has become the de facto standard that NOAA uses for identifying El Niño (warm) and La Niña (cool) events in the tropical Pacific. It is the running 3-month mean SST anomaly for the Niño 3.4 region (i.e., 5° N–5° S, 120°–170° W). Events are defined as five consecutive months at or above the +0.5° anomaly for warm (El Niño) events and at or below the −0.5° anomaly for cold (La Niña) events. The threshold is further broken down into weak (with a 0.5 to 0.9 SST anomaly), moderate (1.0 to 1.4), and strong (≥1.5) events (http://ggweather.com/enso/oni.htm).

In order to monitor ENSO by basing the multivariate ENSO Index (MEI) on the six main observed variables over the tropical Pacific. These six variables are: sea level pressure (P), zonal (U), and meridional (V) components of the surface wind, sea surface temperature (S), surface air temperature (A), and total cloudiness fraction of the sky (C). These observations have been collected and published in Comprehensive Ocean–Atmosphere Data Set (COADS) for many years. The MEI is computed separately for each of 12 sliding bimonthly seasons (Dec/Jan, Jan/Feb,…, Nov/Dec). After spatially filtering the individual fields into clusters (Wolter 1987), the MEI is calculated as the first unrotated principal component (PC) of all six observed fields combined. This is accomplished by normalizing the total variance of each field first and then performing the extraction of the first PC on the covariance matrix of the combined fields (Wolter and Timlin 1993). In order to keep the MEI comparable, all seasonal values are standardized with respect to each season and to the 1950–1993 reference period. The MEI is extended during the first week of the following month based on near-real-time marine ship and buoy observations summarized into COADS-compatible 2-degree monthly statistics at NOAA-ESRL PSD. Negative values of the MEI represent the cold ENSO phase, a.k.a. La Niña, while positive MEI values represent the warm ENSO phase (El Niño; http://www.cdc.noaa.gov/people/klaus.wolter/MEI).

References

Amador JA, Alfaro EJ, Lizano OG, Magaña VO (2006) Atmospheric forcing of the eastern tropical Pacific: a review. Prog Oceanogr 69:101–142

Beier E, Ripa R (1999) Seasonal gyres in the Northern Gulf of California. J Phys Oceanogr 29:305–311

Brown J, Colling A, Park D, Phillips J, Rothery D, Wright J (1989) Ocean circulation. The Open University, Oxford

Cabrera-Ramos CE (2005) Monitoreo Satelital de la Superficie del Océano y su Aplicación en Cruceros Oceanográficos. Universidad Autónoma de Baja California, Ensenada

Carrillo LE, Lavín MF, Palacios-Hernández E (2002) Seasonal evolution of the geostrophic circulation in the Northern Gulf of California. Estuar Coast Shelf Sci 54:153–173

Curry JA, Webster P (1999) Thermodynamics of atmospheres and oceans. Academic, San Diego

da Silva A, Young AC, Levitus S (1994) Atlas of surface marine data, vol 1: algorithms and procedures. NOAA Atlas NESDIS 6, US Department of Commerce, Washington, DC

Delgadillo-Macías J, Aguilar-Ortega T, Rodríguez-Velásquez D (1999) Los aspectos económicos y sociales de El Niño, Capítulo 6. In: Magaña VO (ed) Los impactos de El Niño en México. Dirección General de Protección Civil. Secretaría de Gobernación, Mexico City, pp 181–212

Enfield DB (1996) Relationships of inter-American rainfall to tropical Atlantic and Pacific SST variability. Geophys Res Lett 23:3505–3508

Enfield DB, Mayer MA (1997) Tropical Atlantic SST variability and its relation to "El Niño/Southern Oscillation". J Geophys Res 102:929–945

ERIC (1996) Extractor Rápido de Información Climatológica, ERIC. Instituto Mexicano de Tecnología del Agua, Morelos, Mexico. CD-ROM

Fiedler PC, Talley LD (2006) Hydrography of the eastern tropical Pacific: a review. Prog Oceanogr 69:143–180

Fortin J (2002) La Météo Comprendre le climat et l'environnement (edited by Fortín Jacques). QA International, Québec Canada, p 71

Gill AE (1982) Atmosphere–ocean dynamics. Academic, New York

Hernández B (2002) Variabilidad interanual de las anomalías de la temperatura superficial del mar en aguas cubanas y su relación con eventos El Niño-Oscilación del Sur (ENOS). Investig Mar Valparaiso 30:21–31

Lavín MF, Palacios-Hernández E, Cabrera C (2003) Sea surface temperature anomalies in the Gulf of California. Geofís Int 42:363–375

Lavín MF, Beier E, Gomez-Valdés J, Godínez VM, García J (2006) On the summer poleward coastal current off SW México. Geophys Res Lett 33:L02601. doi:10.1029/2005gl024686

Llunch-Cota SE, Lluch-Belda D, Lluch-Cota S, López-Martínez J, Nevárez-Martínez M, Ponce-Díaz G, Salinas-Zavala G, Vega-Velazquez A, Lara-Lara JR, Hammann G, Morales J (1999) Las pesquerías y El Niño, chapter 5. In: Magaña VO (ed) Los impactos de El Niño en México. Dirección General de Protección Civil. Secretaría de Gobernación, Mexico City, pp 137–180

Martínez RE (2006) Manifestación de El Niño 1997–98 en los Campos de Temperatura y Salinidad en la costa del Pacífico Central Mexicano. Universidad de Guadalajara, MSc thesis, Guadalajara, Jalisco, Mexico

Mestas-Nuñez AM, Miller A (2006) Interdecadal variability and climate change in the eastern tropical Pacific: a review. Prog Oceanogr 69(2–4):267–284

Meza RS (2006) Variabilidad espacio-temporal de la temperatura superficial del mar en el caribe. MSc thesis, Universidad de Guadalajara, Guadalajara, Jalisco, Mexico

Palacios-Hernández E (2001) Circulación de la Región del Golfo de California: estacional y anomalías. Doctoral thesis, Departamento de Oceanografía Física, Centro de Investigación Científica y de Educación Superior de Ensenada, Ensenada, B.C., Mexico, 42 pp

Palacios-Hernandez E, Argote-Espinosa ML, Amador-Buenrostro A, Mancilla-Peraza M (1996) Simulación de la circulación barotrópica inducida por viento en Bahía Sebastián Vizcaino, B. C. Atmósfera 9:171–188

Palacios-Hernandez E, Beier E, Lavín MF, Ripa P (2002) The effect of the seasonal variation of stratification on the circulation of the Northern Gulf of California. J Phys Oceanogr 32:702–728

Palacios-Hernández E, Carrillo L, Lavín MF, Zamudio L, García-Sandoval A (2006) Hydrography and circulation in the Northern Gulf of California during winter of 1994–1995. Cont Shelf Res 26:82–103

PROFEPA (1995) Mortandad de mamiferos y aves marinas en el Alto Golfo de California Final Report. Procuraduría Federal de Protección al Ambiente (PROFEPA), 40 pp

Ripa P (2002) Least squares data fitting. Cienc Mar 28:79–105

Salinas-Zavala CA, Lluch-Cota DB, Hernández-Vázquez S, Lluch-Cota D (1992) Anomalías de precipitación en Baja California Sur durante 1990. Posibles causas. Atmósfera 5:79–93

Shea DJ, Trenberth KE, Reynolds RW (1992) A global monthly sea surface temperature climatology. J Climate 5:987–1001

Trasviña A, Lluch-Cota D, Filonov AE, Gallegos A (1999) Los impactos de EL Niño en México, Cap. 3, pags. 69–103. Universidad Nacional Autónoma de México/InterAmerican Institute for the Global Change Research/Secretaría de Gobernación/Secretaría de Educación Pública-Consejo Nacional de Ciencia y Tecnología

Turrent C, Cavazos T (2009) Role of the land–sea thermal contrasts in the interannual modulation of the North American Monsoon. Geophys Res Lett 36:L02808. doi:10.1029/2008GL036299

Wang C, Fiedler PC (2006) ENSO variability and the Eastern Tropical Pacific: a review. Prog Oceanogr 69(2–4):239–266

Wolter K (1987) The Southern Oscillation in surface circulation and climate over the tropical Atlantic, Eastern Pacific, and Indian Oceans as captured by cluster analysis. J Clim Appl Meteorol 26:540–558

Wolter K, Timlin MS (1993) Monitoring ENSO in COADS with a seasonally adjusted principal component index. Proceedings of the 17th Climate Diagnostics Workshop, Norman, OK, NOAA/NMC/CAC, NSSL, Oklahoma Clim. Survey, CIMMS and the School of Meteorology, University of Oklahoma, pp 52–57

Wyrtki K (1964) The thermal structure of the eastern Pacific Ocean. Deutschen Hydrographischen Zeitschrift, Ergänzungsheft A 6:84

Wyrtki K (1965a) Surface currents of the eastern tropical Pacific Ocean. Inter-American Tropical Tuna Commission Bulletin 9:271–304

Wyrtki K (1965b) Summary of the physical oceanography of the Eastern Pacific Ocean. University of California, Institute of Marine Resources, Ref. 65–10. UCSD-34P99-11, 69 pp

Wyrtki K (1966) Oceanography of the eastern equatorial Pacific Ocean. Oceanogr Mar Biol Annu Rev 4:33–68

Wyrtki K (1967) Circulation and water masses in the eastern equatorial Pacific Ocean. Int J Oceanol Limnol 1:117–147

Zamudio L, Hulburt HE, Metzger EJ, Tilburg CE (2007) Tropical wave-induced oceanic eddies at Cabo Corrientes and the María Islands, México. J Geophys Res 112:C05048. doi:10.1029/2006JC004018

Zuidema P, Fairall Ch, Hartten LM, Hare JE, Wolfe D (2007) On air–sea interaction at the mouth of the Gulf of California. J Clim 20:1649–1661